IEEE Access
Multidisciplinary | Rapid Review | Open Access Journal

Received July 19, 2020, accepted July 28, 2020, date of publication July 31, 2020, date of current version August 13, 2020.

Digital Object Identifier 10.1109/ACCESS.2020.3013539

Developing the First mmWave Fully-Connected Hybrid Beamformer With a Large Antenna Array

SOHAIL PAYAMI[1], MOHSEN KHALILY[1], (Senior Member, IEEE), ALI ARAGHI[1], (Senior Member, IEEE), TIAN HONG LOH[2], (Senior Member, IEEE), DAVID CHEADLE[2], KONSTANTINOS NIKITOPOULOS[1], (Senior Member, IEEE), AND RAHIM TAFAZOLLI[1], (Senior Member, IEEE)

[1]Institute for Communication Systems, University of Surrey, Guildford GU2 7XS, U.K.
[2]5G and Future Communications Technology Group, National Physical Laboratory (NPL), Teddington TW11 0LW, U.K.

Corresponding author: Rahim Tafazolli (r.tafazolli@surrey.ac.uk)

This work was supported by NPL, under NPL-Surrey 2017-2020 collaboration Program. The work of Tian Hong Loh and David Cheadle was supported by the 2017–2020 National Measurement System Programme of the U.K. Government's Department for Business, Energy, and Industrial Strategy (BEIS), under Science Theme Reference EMT20.

ABSTRACT Millimeter wave (mmWave) systems with effective beamforming capability play a key role in fulfilling the high data-rate demands of current and future wireless technologies. Hybrid analog-to-digital beamformers have been identified as a cost-effective and energy-efficient solution towards deploying such systems. Most of the existing hybrid beamforming architectures rely on a subconnected phase shifter network with a large number of antennas. Such approaches, however, cannot fully exploit the advantages of large arrays. On the other hand, the current fully-connected beamformers accommodate only a small number of antennas, which substantially limits their beamforming capabilities. In this article, we present a mmWave hybrid beamformer testbed with a fully-connected network of phase shifters and adjustable attenuators and a large number of antenna elements. To our knowledge, this is the first platform that connects two RF inputs from the baseband to a 16× 8 antenna array, and it operates at 26 GHz with a 2 GHz bandwidth. It provides a wide scanning range of 60°, and the flexibility to control both the phase and the amplitude of the signals between each of the RF chains and antennas. This beamforming platform can be used in both short and long-range communications with linear equivalent isotropically radiated power (EIRP) variation between 10 dBm and 60 dBm. In this article, we present the design, calibration procedures and evaluations of such a complex system as well as discussions on the critical factors to consider for their practical implementation.

INDEX TERMS Millimeter wave, multiple-input multiple-output, fully-connected hybrid beamforming, phased array antenna, testbed.

I. INTRODUCTION

New wireless technologies and applications, such as virtual reality and augmented reality, require a high-speed transmission of data over wireless links. As the sub-6 GHz bands are becoming saturated by many wireless technologies, the mobile operators are exploiting large chunks of unlicensed/lightly licensed spectrum that are available in the millimeter wave (mmWave) frequencies. For example, the fifth-generation (5G) providers in the United States and the United Kingdom use 28 GHz and 26 GHz bands, respectively. On the other hand, achieving high data rates at such frequencies is very challenging due to several technical reasons [1]–[3]. First, the signals transmitted over mmWave channels experience significant attenuation due to high path loss [3]–[6]. In addition, mmWave channels only offer limited scattering and reflection of electromagnetic waves [7]. Consequently, there are only a few physical directions that allow a transmitter and a receiver to communicate. Hence, effective beam alignment techniques are necessary to

The associate editor coordinating the review of this manuscript and approving it for publication was Xujie Li.

establish a reliable link between terminals [8]. To overcome such challenges, an antenna array with a large number of elements is needed to electronically steer the directional beams towards desired directions in mmWave systems [9]–[11]. This is achieved by controlling the phase and magnitude of signals at each antenna based on beamforming techniques. In this context, fully-digital systems, with a dedicated radio frequency (RF) chain per antenna, offer significant flexibility and degrees of freedom to apply suitable algorithms. However, the large number of the required RF chains makes digital beamformers an expensive, power-hungry, and bulky solution for mmWave systems.

Analog beamformers, on the other hand, have only a single RF chain and a phased array antenna. They offer hardware simplicity, lower cost and power consumption compared to fully-digital systems. However, analog beamformers, with a single RF chain, cannot provide high orders of spatial multiplexing gain. Hence, the achievable data rates by such systems may be much lower in comparison with fully-digital beamformers. Several independent access points can be used to increase the number of transmit data streams in an area. Practical trials have shown that the system performance can be significantly boosted if joint processing takes place among the analog beamformers [12]. Such studies highlight the need for a third group of beamforming approaches, known as hybrid analog-and-digital beamformers.

In a hybrid beamformer, a small number of RF chains are connected to a large number of antennas via a network of phase shifters [13]–[17]. Compared to analog and digital beamformers, hybrid approaches can offer a tradeoff between spatial multiplexing gain, cost, complexity, and power consumption. As a result, they have been identified as one of the most promising approaches to implement systems that are based on 802.11 ay and 5G new radio. Hybrid beamformers can be divided into subconnected and fully-connected structures, as shown in Figure 1 [2], [18], [19]. Theoretical analysis of different structures has shown that fully-connected hybrid beamformers provide significantly more degrees of freedom to design algorithms and reach higher data rates. However, these systems are much more expensive and complex to build. Hence, most of the existing hybrid beamforming testbeds and products are based on the subconnected approaches [9], [12], [20]–[22].

With this background, we have designed, built, and evaluated a fully-connected hybrid beamformer with 128 antennas and two RF ports that operate at 26 GHz over a 2 GHz bandwidth; which to our knowledge, is the first of its kind in the world. This platform is algorithm-agnostic and it can support various hybrid massive MIMO approaches. In particular, the fully-connected structure of the beamformer allows for implementing hybrid beamforming algorithms which provide higher data rates compared to the subconnected structures. This system provides flexibility to control the phase and magnitude of the signals between each RF chain and antenna via 6-bits resolution phase shifters and 6-bits resolution attenuators. This feature enables the implementation of amplitude tappering techniques to reduce sidelobe levels and, consequently, interference towards undesired directions. The 16×8 structure of the antenna array allows for steering the beams in both azimuth and elevation. The effective isotropic radiated power (EIRP) of the system can linearly vary from 10 dBm up to 60 dBm. The system's high dynamic range allows for the transmission of various waveforms with different modulations over both short-range and long-range communication links. Hence, the developed testbed provides a unique platform for researchers to develop robust hybrid beamforming algorithms for mmWave systems. In the rest of the paper, we present the most important steps that, we believe, will be of great interest to the researchers who aim to build a similar testbed, regardless of the exact dimensions of the antenna array or the center frequency of the system.

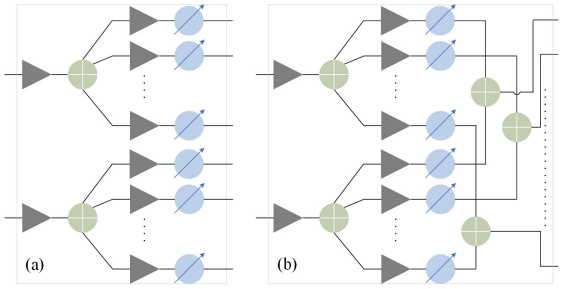

FIGURE 1. Block diagram of (a) subconnected, (b) fully-connected structures.

II. PRIMER: HYBRID BEAMFORMING AND STATE-OF-THE-ART

In this section, we present a brief overview about the design of hybrid beamformers from the both algorithm and implementation points of view. The design of hybrid beamforming algorithms is a challenging task due to the nonconvex constant modulus constraints[1] that are imposed by the phase shifters. In addition, most of the commercial phase shifters are digitally controlled, and they provide discrete set of phase values. As a result, the optimization of hybrid beamforming weights turns into a nonconvex combinatorial problem which can significantly increase the computational complexity of the corresponding algorithms [17]. The design and performance of such methods also depends on the properties of the propagation channel, performance metric, and the structure of the phase shifter network. For example, the sparsity, richness, or the frequency-selectivity of channel matrix channel directly impacts the choice of the hybrid beamforming algorithms [14], [15], [23]. In addition, the hardware connections within the hybrid beamforming network dictate the degrees of freedom and constraints that are available to the algorithm developers. In a subconnected

[1] In mathematical models, a phase shifter provides ϕ rad of phase shift to its input signal by multiplying it with $e^{j\phi}$. As a result, the phase shifters can only change the phase of the signal and not its magnitude. This property is referred to as *constant modulus constraint*, when formulating the optimization problem to design the hybrid beamforming weights [8].

structure, shown in Figure 1 (a), each RF chain is only connected to a subset of antennas. However, in a fully-connected structure, each RF chain is connected to all of the antennas, as shown in Figure 1 (b). The theoretical studies on hybrid beamformers show that fully-connected beamformers can reach significantly higher data rates compared to subconnected approaches [16]. Moreover, the larger number of phase shifters provides more degrees of freedom to design algorithms. Besides, the connection from each RF chain to all of the antennas provides higher array gains to boost the signal-to-noise- ratio (SNR) for each data stream.

From an implementation point of view, fabricating fully-connected beamformers is much more challenging than the subconnected structures. In the full-connected configuration, a large number of electrical components and RF tracks need to be placed in a small physical area. The required proximity gives rise to mutual coupling effects between the RF paths, phase shifters, and antennas. Such issues become even more challenging as the operating frequency of the circuit increases, and the number of the antennas scales up. Hence, most of the implementations of hybrid beamformers are based on subarray structures, such as in [12], [20]–[22] and references therein.

The authors in [12] present a subconnected hybrid beamformer with 32 antennas and 2 RF chains for 60 GHz applications. They show that a subconnected structure with two RF chains and phased arrays significantly outperforms two analog beamformers with the same array size. In other words, despite the directional nature of 60 GHz channels, the cooperation between the two RF chains provides a noticeable performance gain to better improve the signal to interference noise ratio (SINR) for the users. The 64-element phased array of [20] operates at 28 GHz and provides $\pm 50^{\circ}$ scanning range in azimuth and can support EIRP of up to 52 dBm. The 8×1 array of [22] provides a similar scanning range, and its EIRP at the saturation point is around 40 dBm. The 256-element transceiver of [21] is also based on a subconnected structure, and it operates at 60 GHz. A wideband fully-connected hybrid beamformer with 8 antennas and 2 RF inputs for the receiver side at 28 GHz is presented in [24]. Another fully-connected hybrid beamformer for multi-standard MIMO receivers at 28 GHz and 37 GHz with 2 RF ports and 4 antennas is proposed in [25]. However, the array size of [24], [25] may not be sufficient to compensate for high path loss of mmWave channels in many practical scenarios.

In summary, the mmWave systems require a large number of antennas. However, most of the existing hybrid beamformers are based on subconnected structures that cannot fully realize the benefits of large arrays. On the other hand, the existing fully-connected hybrid beamformers have a relatively small number of antennas. With this motivation, we have designed, built, and tested a fully-connected wideband hybrid beamformer with 128 antennas and 2 RF inputs at 26 GHz. In the following, we present the most significant steps that are required to design, implement, and verify this system.

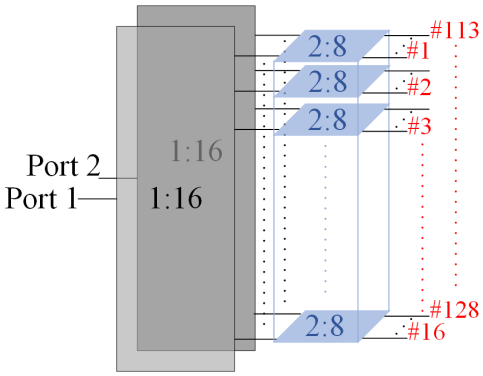

FIGURE 2. Signal distribution scheme across the hybrid beamforming module.

III. DESIGN, CALIBRATION AND TEST PROCEDURES

This section presents an overview of the most important design consideration towards building our testbed. The hybrid beamformer consists of a programmable phase shifter and attenuator network, a cooling system, a control interface to program the phase shifters and attenuators, and a power supply. A Keysight 34980 Multifunction Switch / Measure is used to digitally control the phase shifters and attenuators of the hybrid beamformer from MATLAB on a computer. An Ethernet cable provides the connection between the computer and Keysight 34980, and eight 78-pin Dsub connectors and cables make the connection between Keysight 34980 and the hybrid beamformer. A Keysight N5765 power supply is used to provide the required current and voltage to operate the hybrid beamformer. The rest of this section is mainly focused on the design of the RF front-end and antenna array.

As shown in the diagram of Figure 2, there are two RF inputs to the hybrid beamformer. Each RF input is split into 16 signals, and then passed into a fully-connected beamforming module with two RF inputs and 8 outputs. This system consists of 16×8 antenna array. Figure 3 further depicts the details of the whole system and the 2:8 beamformer modules which consist of a fully-connected network of phase shifters and adjustable attenuators. The outputs of the modules are, then, amplified and and fed to the antennas. It is noted that Figure 2 and Figure 3 present the block diagram of the same system, with a 90 degrees rotation in the viewing angle. In the following, we explain the design and test procedures of different blocks of Figure 3 in detail.

A. POWER SPLITTER NETWORK

A 1-to-16 Wilkinson power splitter network has been designed, shown in Figure 4, to divide each of the two input signals of the hybrid beamformer among the 16 beamforming modules. This passive network is placed at the very beginning stage of the hybrid beamformer (see Figure 3). Comparing

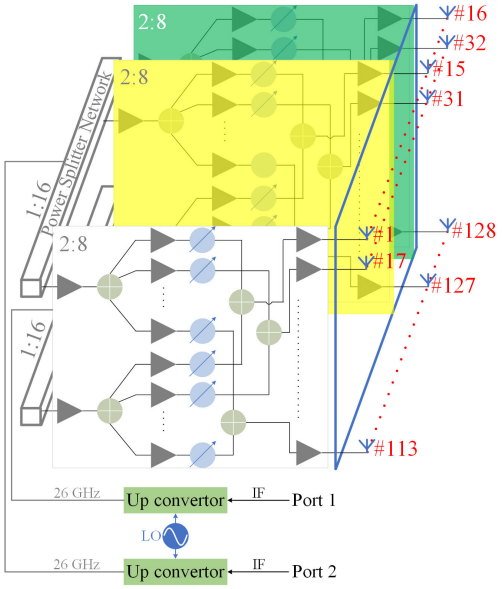

FIGURE 3. Detailed block diagram of the hybrid beamforming module.

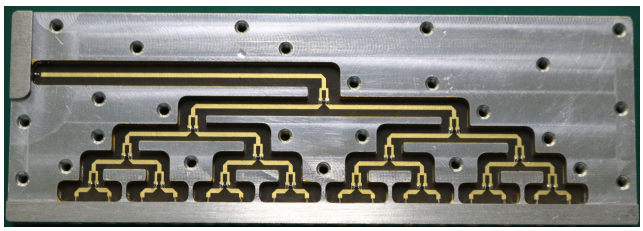

FIGURE 4. 1:16 power splitter network.

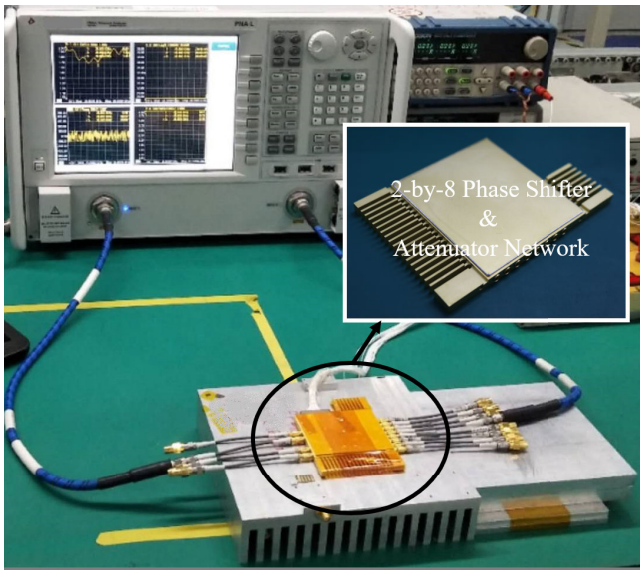

FIGURE 5. Beamforming module with 2 RF inputs and 8 outputs.

to conventional network dividers, Wilkinson offers higher isolation between adjacent arms in a relatively compact size. The compact size of network is an important factor to reduce the signal losses, especially in the mmWave bands. This is due to the fact that the signal attenuation is related to the length of the transmission lines; as the length of the lines reduces, so does the signal attenuation. An Agilent 5244 vector network analyzer (VNA) is used to evaluate the functionality of the designed power splitter. Compared to our design specifications, the key requirements and measured values are summarized as:

- The total loss per channel should be less than 18 dB, the maximum loss that we measured was 17.96 dB;
- Isolation between channels should be greater than 20 dB, we achieved 21.9 dB in the worst case;
- Input Voltage Standing Wave Ratio (VSWR) should be lower than 1.6:1, we achieved maximum of 1.33;
- Output VSWR should be lower than 1.6:1, we achieved a maximum of 1.49.

In general, the input signal level of a power splitter decreases at its output based on two factors: nominal loss and insertion loss. For an N-way Wilkinson power splitter, the nominal loss is defined as $10\log_{10} N$ dB. The insertion loss mainly originates from dielectric and conductive loss of the transmission line, the fabrication and installation issues. In practice, a well-designed structure can only minimize insertion loss, and not eliminate it. In our designed Wilkinson power splitter, the traveling wave on the microstrip line is divided by two subpath for four times to form a 1-to-16 divider. In an ideal case, the signal level drops by $10\log_{10} 16 = 12$ dB. During our measurements, we observed 17.96 dB total loss in the worst-case scenario, which indicates that the insertion loss of the splitter is 5.96 dB. Hence, our designed power divider, with a significantly lower implementation cost than of industrialized commercial products, e.g., [26], [27], provides high efficiency and meets our system requirements.

B. PHASE SHIFTING AND ATTENUATION

The fully-connected phase shifter and attenuator network consists of 256 programmable phase shifters and attenuators which are equally distributed among 16 modules. The outputs of these beamforming modules will then be amplified before they are fed to the antennas (see Figure 3). Each module consists of two RF inputs and eight outputs that are connected by 16 phase shifters and 16 attenuators, as shown in Figure 5. Each phase shifter can select an arbitrary combination of the values in $\{0, 5.625°, 11.25°, 22.5°, 45°, 90°, 180°\}$ by using 6 control-bits. As a result, there are 2^6 phase combinations, and the theoretical phase resolution is 5.625°. The relationship between each phase shifter's control-bits $\{b_0, b_1, b_2, \ldots, b_5\}$ and the corresponding phase value $\theta°$ is

$$\theta° = b_0 \times 5.625° + b_1 \times 11.25° + b_2 \times 22.5° + b_3 \times 45° + b_4 \times 90° + b_5 \times 180°. \quad (1)$$

Similarly, the attenuators can select an arbitrary combination of attenuation levels from the set $\{0, 0.5, 1, 2, 4, 8, 12\}$ dB by using 6 control-bits.

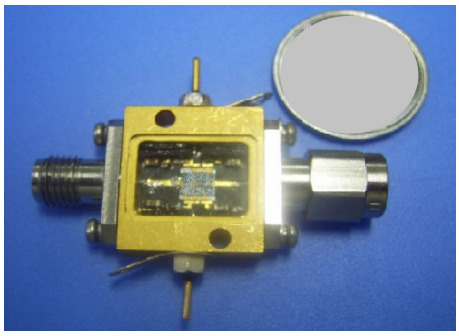

FIGURE 6. Prototype of the power amplifier.

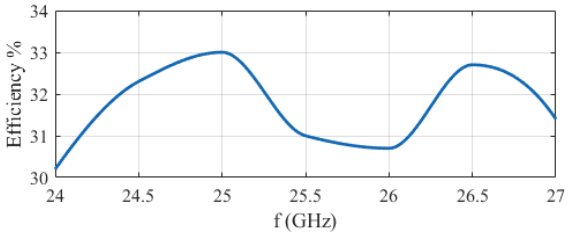

FIGURE 7. Power amplifier efficiency test curve, where drain and gate voltages are set as $V_d = 6$v, $V_g = -0.7$v, respectively.

After the fabrication and testing of the modules, We observed around 5 degrees phase-shifting error and around 0.5 dB attenuation error when comparing the theoretical targets with the measured values. We identified the following reasons for this observation. First, the overall error in the whole system cannot be smaller than the error associated with each components. We used commercial off-the-shelf chips for the phase shifters and attenuators. The root mean square (RMS) error of each of the chips is about 2.5° for the phase shifters and 0.3 dB for the attenuators. Second, we observed some deterioration in the pins of the phase shifter and attenuator chips after fabrication. Due to the high frequency of operation, the grounding performance of the chips and the matching state between the chips had slightly changed during the assembly process. This, in turn, affected the precision of phase shifters and attenuators. Despite the observed difference between theoretical and measured values, it will be shown in subsection III-F that such deviations do not have a significant impact on the overall performance of the beamformer. This is due to the fact that the random errors from a large number of phase shifters and attenuators are averaged out before the antennas.

C. POWER AMPLIFIER

To deploy the designed hybrid beamformer in both short-distance and long-distance mmWave communication scenarios, it is necessary for the beamformer to linearly provide a wide range of power levels. This linearity and the total EIRP of the system in this design are decided by the last stage power amplifiers. For RF power amplifiers, there is always a trade-off between efficiency and linearity. For our purposes, the linearity of the amplifiers has a higher priority as it guarantees the fidelity of the system's response versus different signal levels. The efficiency of the power amplifier plays a significant role in the total power budget of the system's front-to-end. Based on these considerations, we set the minimum requirement for the efficiency to at least 30% for the entire band that the amplifier's performance is linear. A prototype of the power amplifier and its measured efficiency are shown in Figures 6 and 7, respectively. As it is observed, it has a very small size which is comparable to a coin with an acceptable efficiency, between 30.1% to 33%, over the entire band of interest. A VNA is used to test the functionality and performance of the power amplifiers. Compared to the design specifications, the results are reported as:

- Saturation point should be higher than 27 dBm, the measured value was 27.5 dBm;
- P1dB output power greater than 26 dBm, the measured value was 26.7 dBm;
- The third-order intermodulation distortion (IMD3) should be greater than 18 dBc, our measurement was 18.5∼27dBc.

D. CALIBRATION

After fabrication and assembly of the splitters, beamforming modules, and power amplifiers, it is necessary to calibrate the corresponding phases and amplitudes at the output of the system. The calibration is performed before connecting the antennas to the rest of testbed. This is a time-consuming process which needs to be repeated for all the phase and amplitude values form {5.625°, 11.25°, 22.5°, 45°, 90°, 180°} and {0, 0.5, 1, 2, 4, 8, 12} dB and for all of the 256 phase shifters and attenuators. A VNA is used to measure the phase and amplitude difference between each RF input of the hybrid beamformer and the antenna ports, i.e., the output of the phase shifter and attenuator network. Since the antennas are not connected at this stage, it is necessary to terminate all the ports, except the port under calibration, with a 50 Ohm termination. This step is critical as the ports which are not terminated appropriately, may reflect signals back to the power amplifiers. This may cause significant damage to the equipment. The phase calibration has two stages, and consequently, two calibration tables are required. The first table is used to make the phase differences at the antenna ports equal to zero. In other words, this step alleviates the relative phase offsets between different ports and acts as the reference phase value for each phase shifter. Then, the second calibration table is applied to create the required phase shift with respect to the reference value for the corresponding phase shifter. To calibrate the amplitudes, it is only required to measure the attenuation level compared to the designed value. It should be noted that it is not possible to modify the circuit and further improve the performance of the attenuators, at this stage.

E. PHASED ARRAY ANTENNA DESIGN

The air interface of the system consists of a phased array antenna (PHA) which is able to steer a pencil beam towards

the angle of interest. The operating bandwidth is 2 GHz with respect to the centre frequency of $f = 26$ GHz. As it is presented in Figure 3, the proposed PHA contains 128 elements on a 16×8 rectangular lattice with an individual exciting port per element. By regulating the relative phase difference between the ports, the direction of constructed beam can be controlled while the side-lobe-level (SLL) can be managed by controlling the amplitude of each exciting port. Based on the fundamental concepts of PHAs [28], the constructed beam can be expressed by

$$PF = EF \times AF, \tag{2}$$

where PF, EF and AF denote the pattern, element and array factors, respectively. In particular, PF describes the overall characteristics of constructed beam, and EF is each element's radiation pattern. The array factor AF depends on the free-space wavenumber $k = 2\pi/\lambda$, where λ denotes the wavelength, excitation and geometry of the elements of the PHA. For a planar array with $M \times N$ elements, placed on xy plane, the array factor is expressed as [28]

$$AF = I_0 \Big\{ \sum_{m=1}^{M} e^{j(m-1)(kd_x \sin\theta \cos\phi + \beta_x)} \Big\} \times \Big\{ \sum_{n=1}^{N} e^{j(n-1)(kd_y \sin\theta \sin\phi + \beta_y)} \Big\}, \tag{3}$$

where I_0 is the amplitude excitation, d_x (d_y), and β_x (β_y) are the spacing and progressive phase shift between elements along x (y) direction respectively. In order to steer the beam towards $\theta = \theta_0$ and $\phi = \phi_0$, the progressive phase shift must be equal to

$$\begin{aligned} \beta_x &= -kd_x \sin\theta_0 \cos\phi_0 \\ \beta_y &= -kd_y \sin\theta_0 \sin\phi_0, \end{aligned} \tag{4}$$

As mentioned, the proposed PHA structure is composed of 128 elements as presented in Figure 8. Each element is a hat-shaped printed patch antenna excited by a single coaxial port, as shown in Figure 8 (a) and (b). The substrate is Rogers RO4003C with $\epsilon_r = 3.55$, $\tan\delta = 0.0027$ and thickness of $h = 0.813$ mm. Each connector is a standard mmWave SMP attached to a 2.92 mm female adapter. The optimized geometrical dimensions of each element at the presence of its corresponding connector are $d_1 = 3.3$ mm, $d_2 = 1$ mm, $d_3 = 1.78$ mm, $d_4 = 0.68$ mm. It should be noted that the impedance matching is controlled by parameter d_4 while d_1, d_2, and d_3 impact the reactive loads of the patch [29], [30], and therefore regulate the operating bandwidth. The array configuration is presented in Figure 8 (c) with the overall substrate sheet dimensions of $d_5 = 95$ mm and $d_6 = 48.6$ mm. Considering λ_0 as the wavelength of centre frequency, the spacing between elements is set to be $\lambda_0/2$, which is $d_7 = 5.8$ mm. Figure 8 (d) shows the fabricated prototype array antenna in an anechoic chamber room.

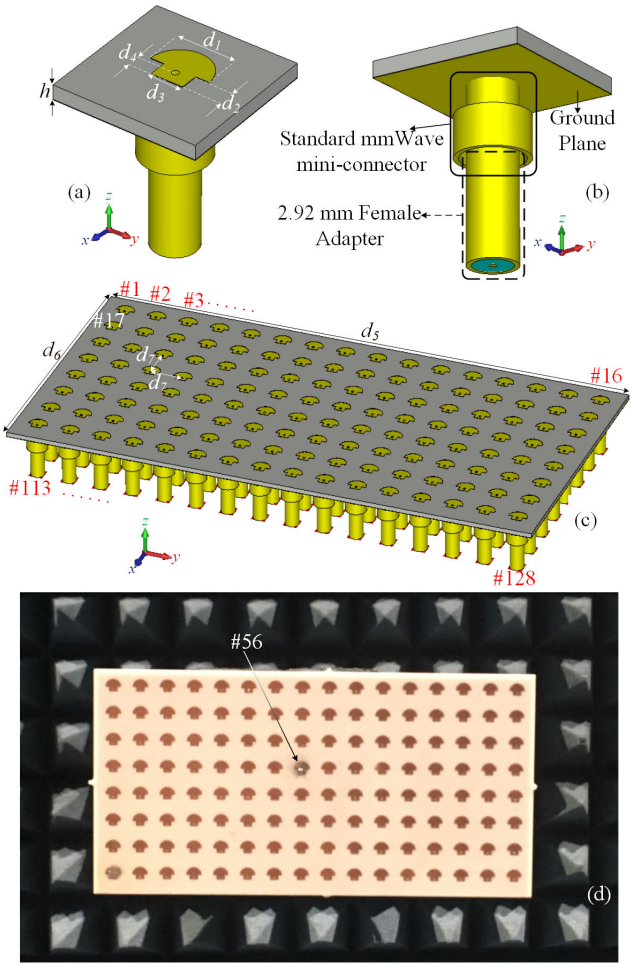

FIGURE 8. The proposed antenna, (a) single element top view, (b) single element back view, (c) array configuration, (d) fabricated prototype in the anechoic chamber.

F. SIMULATED RESULTS AND MEASUREMENTS

The proposed structure is analyzed by the full-wave software CST-MWS. The simulated scattering parameters (S-parameters) of the designed structure are presented in Figure 9. Based on our analytical studies, it is important to note that the resonance frequency of each antenna element shifts down by around 300 MHz, when all of the elements are placed adjacent to each other and form an array. Consequently, we included the impact of this observation in the dimensions of every single element. In other words, each antenna is designed such that it resonates at 26.3 GHz, as shown in Figure 9 (a). Figure 9 (b) presents the S-parameters for several antenna locations over the lattice, once forming an array of elements. It is observed that the PHA's elements resonate at the desired 26 GHz frequency, and the bandwidth of each element is more than 2 GHz (1 GHz) with respect to -10 dB (-15 dB) margin. In addition, the maximum cross coupling level for the adjacent elements is less than -15 dB across the operating band. Figures 10 (a) and (b) present the simulated radiation pattern of single-elements as well as the PHA. With $+90$deg (-90deg) progressive phase difference between the elements

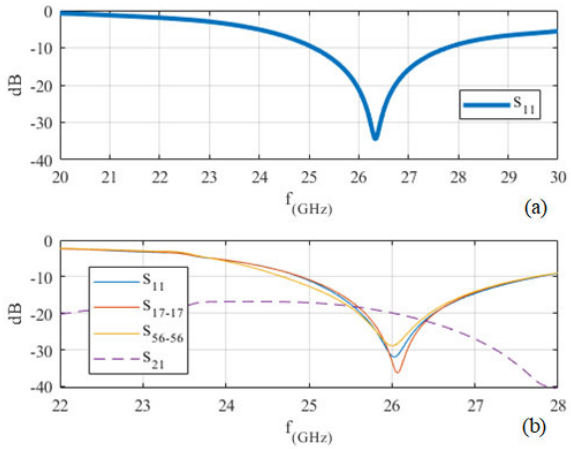

FIGURE 9. The S-parameters. (a) single element, (b) the performance of elements #1, #17, #56 in the array configuration.

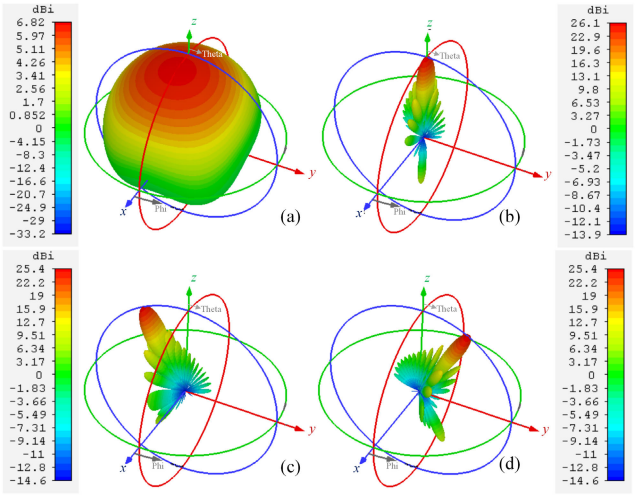

FIGURE 10. The simulated radiation pattern at $f = 26$ GHz, (a) single element, (b) PHA, (c) -30 deg scanned angle on H-plane, (d) 30 deg scanned angle on H-plane.

along the $y-$axis, see Figure 8 (c) and Eq. 4, the PHA's H-plane beam can be tilted by -30 deg ($+30$ deg) as presented in Figure 10 (c) and (d). As an example for the performance of a single element that is placed in the antenna array, consider the centrally located #56 in Figure 8 (d). The measured S-parameter is presented in Figure 11 (a), and it clearly shows that the fabricated antenna is well matched at the frequency of interest. The measured radiation pattern of the corresponding antenna is illustrated in Figure 11 (b).

Based on the block-diagram of the hybrid beamformer, shown in Figure 3, the fabricated array antenna is attached to the front-to-end and controlling system, as depicted in Figure 12. A conventional array can achieve SLL ≥ -13 dB. Based on our link-budget analysis, the required SLL for some scenarios is less than -15 dB. To further reduce the SSL, Taylor amplitude tapering has been applied on the array's elements to achieve SLL≈ -20 dB. Since the attenuators in the front-to-end system have a limited number of discrete

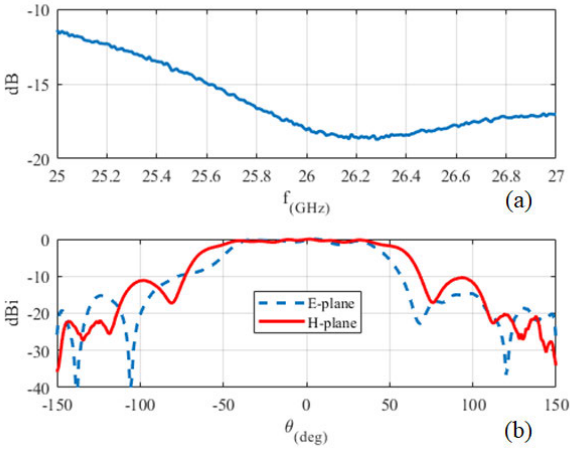

FIGURE 11. The measured results of a single antenna element, (a) S-parameter, (b) radiation pattern.

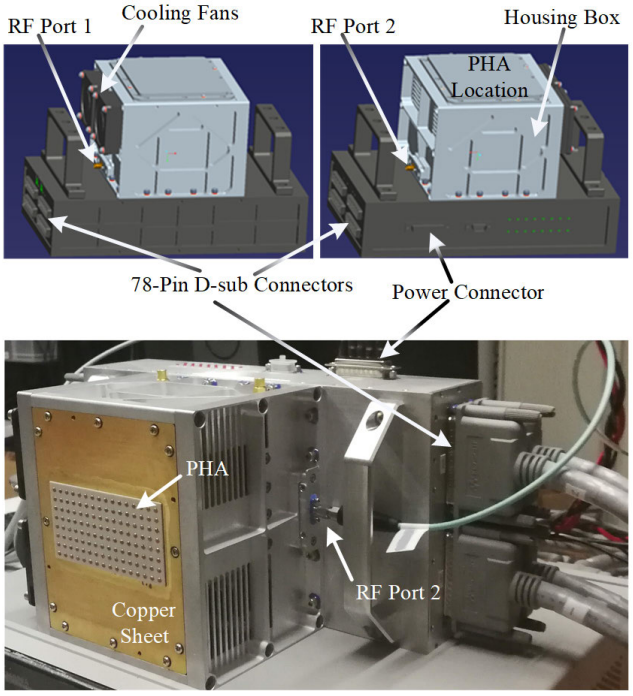

FIGURE 12. The fully implemented hybrid beamformer.

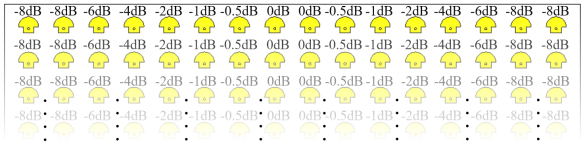

FIGURE 13. The applied rounded amplitudes per antenna element.

states, the desired Taylor distribution has been rounded to the closest values that would be obtainable by the attenuators. The rounded values that have been applied in the array are presented in Figure 13.

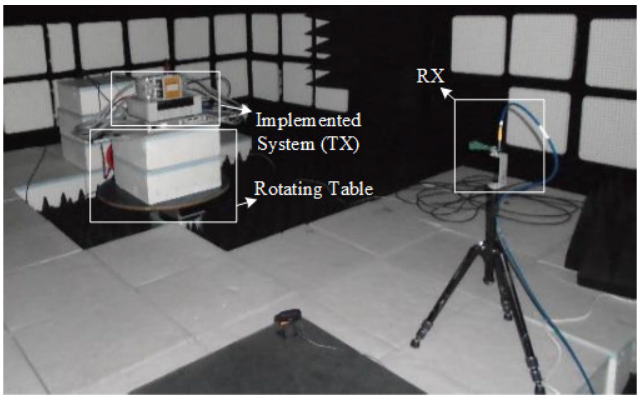

FIGURE 14. System performance measurement setup.

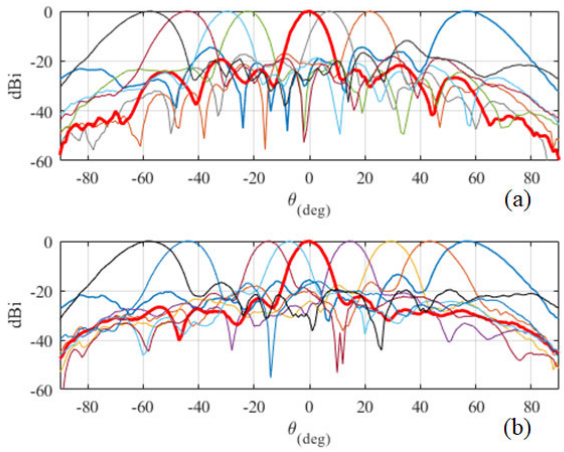

FIGURE 15. The measured H-plane radiation pattern at $f = 26$ GHz for different values of tilt angle, (a) Port 1, (b) Port 2.

The performance of the testbed has been assessed via the measurement setup presented in Figure 14. The measured H-plane radiation patterns for different tilt angles of $-60 \sim +60$ deg are presented in Figure 15 for both Ports 1 and 2. As it is clear from this figure, the required SLL of -15 dB is well achieved for the boresight scenario. The highest SLL of -16 dB is occurred for the tilt angle of ± 60 deg which is still acceptable from a link-budget point of view for many scenarios.

Considering Figure 10 (a) and Figure 11 (b), the designed antenna element provides an EF with a relatively wide H-plane beam without significant fluctuations over $-60 < \theta < 60$. As a result, the constructed PF, see Eq. 2, of the proposed PHA is capable of tilting the beam to around ± 60 deg. It is noted that the steered beam has neither distorted the pattern, nor imposed a severe scanning loss, as shown in Figure 10 (c, d) and Figure 15. To the best of our knowledge, such a wide-scanning range in the 26 GHz band has not been reported before for such a large array.

IV. CONCLUSION AND FUTURE DIRECTIONS

This paper presented an overview of the design, calibration, and test procedures towards building the first mmWave fully-connected hybrid beamformer with 128 antennas and two input signals from two RF chains at 26 GHz. This system offers significant advantages and increased flexibility compared to state-of-the-art hybrid beamformers. The two RF inputs and the 16×8 structure of the antenna array allow for steering two pencil beams in both azimuth and elevation. In addition, the ability to control the amplitude of the signals at each antenna element provides better control over the sidelobe levels. The fully-connected structure of the beamformer paves the path to develop, implement, and test a plethora of hybrid beamforming algorithms, which are not realizable with a conventional subconnected configuration. Despite the abundant literature on designing algorithms for hybrid beamformers, refer to the survey papers [31], [32], most of the existing work relies on theoretical assumptions about the hardware constraints and the propagation channels. The performance of such algorithms may significantly vary according to the propagation scenario, and the hardware design. The high dynamic range of the EIRP of our developed beamformer gives us the opportunity to deploy it in various scenarios. Consequently, we can design, evaluate, and validate advanced transmission approaches for channel estimation, beam alignment, and beamforming algorithms that are tailored to realistic transmission scenarios and hardware constraints. In addition, the linearity, high bandwidth and dynamic range of the system enables the beamformer to transmit various waveforms and modulations, such as orthogonal frequency-division multiplexing (OFDM), filtered-OFDM (F-OFDM) and generalized frequency division multiplexing (GFDM).

The designed beamformer can also be used to further optimize the transmission over frequency-selective channels [14], [33], and provide tradeoffs between diversity and spatial multiplexing gains. Such studies may even motivate the deployment of hybrid beamformers in lower frequency bands, which are generally more frequency-selective. In addition, our programmable fully-connected hybrid beamformer with 128 antennas can create semi-omnidirectional and pencil beams. As a result, the effective channel, that is observed at the baseband, and corresponding algorithms can significantly vary. Using wider beams may necessitate the use of more complex nonlinear algorithms, such as [34]–[36], whereas the pencil beams can convert the effective channel into an additive white Gaussian noise channel, and simplify the required processing at the transmitter and receiver.

Another research direction that has recently received significant interest from academia and industry is applying machine learning-based techniques for channel estimation, beam alignment, and calculating the hybrid beamforming weights for mmWave systems [37], [38]. At least, in theory, such approaches seem very appealing as they can enable the transceivers to learn about the environment and adapt to new conditions. However, to the best of our knowledge, the machine leaning-based solutions are built based on computer-based models. Although such results seem very promising, they need to be tailored to real-life scenarios. With this motivation, we are aiming to exploit our testbed to further

explore the application of machine learning-based algorithms in channel estimation and beam alignment in hybrid beamforming systems over realistic mmWave channels.

ACKNOWLEDGMENT

The authors would like to thank support of University of Surrey 5GIC (http://www.surrey.ac.uk/5gic) for this work.

REFERENCES

[1] S. K. Saha, H. Assasa, A. Loch, N. M. Prakash, R. Shyamsunder, S. Aggarwal, D. Steinmetzer, D. Koutsonikolas, J. Widmer, and M. Hollick, "Fast and infuriating: Performance and pitfalls of 60 GHz WLANs based on consumer-grade hardware," in *Proc. 15th Annu. IEEE Int. Conf. Sens., Commun., Netw. (SECON)*, Jun. 2018, pp. 1–9.

[2] W. Roh, J.-Y. Seol, J. Park, B. Lee, J. Lee, Y. Kim, J. Cho, K. Cheun, and F. Aryanfar, "Millimeter-wave beamforming as an enabling technology for 5G cellular communications: Theoretical feasibility and prototype results," *IEEE Commun. Mag.*, vol. 52, no. 2, pp. 106–113, Feb. 2014.

[3] T. S. Rappaport, G. R. MacCartney, M. K. Samimi, and S. Sun, "Wideband millimeter-wave propagation measurements and channel models for future wireless communication system design," *IEEE Trans. Commun.*, vol. 63, no. 9, pp. 3029–3056, Sep. 2015.

[4] M. Khalily, S. Taheri, S. Payami, M. Ghoraishi, and R. Tafazolli, "Indoor wideband directional millimeter wave channel measurements and analysis at 26 GHz, 32 GHz, and 39 GHz," *Trans. Emerg. Telecommun. Technol.*, vol. 29, no. 10, Oct. 2018, Art. no. e3311.

[5] M. Khalily, M. Ghoraishi, S. Taheri, S. Payami, and R. Tafazolli, "Millimeter-wave directional path loss models in the 26 GHz, 32 GHz, and 39 GHz bands for small cell 5G cellular system," in *Proc. 12th Eur. Conf. Antennas Propag. (EuCAP)*, 2018, pp. 1–5.

[6] M. Khalily, M. Ghoraishi, S. Taheri, S. Payami, and R. Tafazolli, "Polarimetric wideband directional channel measurement and analysis for outdoor small cell scenarios at 32 GHz and 39 GHz," in *Proc. 12th Eur. Conf. Antennas Propag. (EuCAP)*, 2018, pp. 1–5.

[7] S. Payami, M. Khalily, S. Taheri, K. Nikitopoulos, and R. Tafazolli, "Channel measurement and analysis for polarimetric wideband outdoor scenarios at 26 GHz: Directional vs omni-directional," in *Proc. 14th Eur. Conf. Antennas Propag. (EuCAP)*, Mar. 2020, pp. 1–5.

[8] R. W. Heath, N. Gonzalez-Prelcic, S. Rangan, W. Roh, and A. M. Sayeed, "An overview of signal processing techniques for millimeter wave MIMO systems," *IEEE J. Sel. Topics Signal Process.*, vol. 10, no. 3, pp. 436–453, Apr. 2016.

[9] S. K. Saha, D. Uvaydov, J. M. Jornet, E. Knightly, D. Koutsonikolas, D. Pados, Z. Sun, Y. Ghasempour, M. K. Haider, T. Siddiqui, P. De Melo, N. Somanchi, L. Zakrajsek, A. Singh, and O. Torres, "x60: A programmable testbed for wideband 60 GHz WLANs with phased arrays," in *Proc. 11th Workshop Wireless Netw. Testbeds, Experim. Eval. CHaracterization WiNTECH*, 2017, pp. 75–82, doi: 10.1145/3131473.3131479.

[10] Y. Ghasempour, M. K. Haider, C. Cordeiro, D. Koutsonikolas, and E. Knightly, "Multi-stream beam-training for mmWave MIMO networks," in *Proc. 24th Annu. Int. Conf. Mobile Comput. Netw. MobiCom*, 2018, pp. 225–239, doi: 10.1145/3241539.3241556.

[11] B. Sadhu, A. Paidimarri, M. Ferriss, M. Yeck, X. Gu, and A. Valdes-Garcia, "A 128-element dual-polarized software-defined phased array radio for mm-wave 5G experimentation," in *Proc. 2nd ACM Workshop Millim. Wave Netw. Sens. Syst. mmNets*, 2018, pp. 21–25, doi: 10.1145/3264492.3264506.

[12] S. Blandino, G. Mangraviti, C. Desset, A. Bourdoux, P. Wambacq, and S. Pollin, "Multi-user hybrid MIMO at 60 GHz using 16-antenna transmitters," *IEEE Trans. Circuits Syst. I, Reg. Papers*, vol. 66, no. 2, pp. 848–858, Feb. 2019.

[13] S. Payami, M. Khalily, T. H. Loh, and K. Nikitopoulos, "Hybrid beamforming with switches and phase shifters over frequency-selective channels," *IEEE Wireless Commun. Lett.*, early access, Apr. 21, 2020, doi: 10.1109/LWC.2020.2989224.

[14] S. Payami, M. Sellathurai, and K. Nikitopoulos, "Low-complexity hybrid beamforming for massive MIMO systems in frequency-selective channels," *IEEE Access*, vol. 7, pp. 36195–36206, 2019.

[15] S. Payami, M. Ghoraishi, and M. Dianati, "Hybrid beamforming for large antenna arrays with phase shifter selection," *IEEE Trans. Wireless Commun.*, vol. 15, no. 11, pp. 7258–7271, Nov. 2016.

[16] S. Payami, M. Ghoraishi, M. Dianati, and M. Sellathurai, "Hybrid beamforming with a reduced number of phase shifters for massive MIMO systems," *IEEE Trans. Veh. Technol.*, vol. 67, no. 6, pp. 4843–4851, Jun. 2018.

[17] S. Payami, M. Shariat, M. Ghoraishi, and M. Dianati, "Effective RF codebook design and channel estimation for millimeter wave communication systems," in *Proc. IEEE Int. Conf. Commun. Workshop (ICCW)*, Jun. 2015, pp. 1226–1231.

[18] S. Payami, C. Masouro, and M. Sellathurai, "Low-complexity and robust quantized hybrid beamforming and channel estimation," in *Proc. IEEE Global Commun. Conf. (GLOBECOM)*, Dec. 2018, pp. 1–6.

[19] S. Payami, N. M. Balasubramanya, C. Masouros, and M. Sellathurai, "Phase shifters versus switches: An energy efficiency perspective on hybrid beamforming," *IEEE Wireless Commun. Lett.*, vol. 8, no. 1, pp. 13–16, Feb. 2019.

[20] K. Kibaroglu, M. Sayginer, T. Phelps, and G. M. Rebeiz, "A 64-element 28-GHz phased-array transceiver with 52-dBm EIRP and 8–12-Gb/s 5G link at 300 meters without any calibration," *IEEE Trans. Microw. Theory Techn.*, vol. 66, no. 12, pp. 5796–5811, Dec. 2018.

[21] U. Kodak, B. Rupakula, S. Zihir, and G. M. Rebeiz, "60-GHz 64- and 256-element dual-polarized dual-beam wafer-scale phased-array transceivers with reticle-to-reticle stitching," *IEEE Trans. Microw. Theory Techn.*, vol. 68, no. 7, pp. 2745–2767, Jul. 2020.

[22] J. Pang *et al.*, "A 28-GHz CMOS phased-array transceiver based on LO phase-shifting architecture with gain invariant phase tuning for 5G new radio," *IEEE J. Solid-State Circuits*, vol. 54, no. 5, pp. 1228–1242, May 2019.

[23] O. E. Ayach, S. Rajagopal, S. Abu-Surra, Z. Pi, and R. W. Heath, "Spatially sparse precoding in millimeter wave MIMO systems," *IEEE Trans. Wireless Commun.*, vol. 13, no. 3, pp. 1499–1513, Mar. 2014.

[24] S. Mondal, R. Singh, A. I. Hussein, and J. Paramesh, "A 25–30 GHz fully-connected hybrid beamforming receiver for MIMO communication," *IEEE J. Solid-State Circuits*, vol. 53, no. 5, pp. 1275–1287, May 2018.

[25] S. Mondal and J. Paramesh, "A reconfigurable 28-/37-GHz MMSE-adaptive hybrid-beamforming receiver for carrier aggregation and multi-standard MIMO communication," *IEEE J. Solid-State Circuits*, vol. 54, no. 5, pp. 1391–1406, May 2019.

[26] *Panda Microwave*. [Online]. Available: https://pandamw.com/

[27] *Mini-Circuits*. [Online]. Available: https://www.minicircuits.com/

[28] C. A. Balanis, *Antenna Theory: Analysis and Design*. Hoboken, NJ, USA: Wiley, 2005.

[29] A. Araghi and G. Dadashzadeh, "Detail-oriented design of a dual-mode antenna with orthogonal radiation patterns utilizing theory of characteristic modes," *ACES J.*, vol. 28, no. 10, pp. 952–955, 2013.

[30] A. Araghi and G. Dadashzadeh, "Oriented design of an antenna for MIMO applications using theory of characteristic modes," *IEEE Antennas Wireless Propag. Lett.*, vol. 11, pp. 1040–1043, 2012.

[31] I. Ahmed, H. Khammari, A. Shahid, A. Musa, K. S. Kim, E. De Poorter, and I. Moerman, "A survey on hybrid beamforming techniques in 5G: Architecture and system model perspectives," *IEEE Commun. Surveys Tuts.*, vol. 20, no. 4, pp. 3060–3097, 4th Quart., 2018.

[32] A. F. Molisch, V. V. Ratnam, S. Han, Z. Li, S. L. H. Nguyen, L. Li, and K. Haneda, "Hybrid beamforming for massive MIMO: A survey," *IEEE Commun. Mag.*, vol. 55, no. 9, pp. 134–141, Sep. 2017.

[33] F. Sohrabi and W. Yu, "Hybrid analog and digital beamforming for mmWave ofdm large-scale antenna arrays," *IEEE J. Sel. Areas Commun.*, vol. 35, no. 7, pp. 1432–1443, Jul. 2017.

[34] B. M. Hochwald, C. B. Peel, and A. L. Swindlehurst, "A vector-perturbation technique for near-capacity multiantenna multiuser communication—Part II: Perturbation," *IEEE Trans. Commun.*, vol. 53, no. 3, pp. 537–544, Mar. 2005.

[35] C. B. Peel, B. M. Hochwald, and A. L. Swindlehurst, "A vector-perturbation technique for near-capacity multiantenna multiuser Communication—Part I: Channel inversion and regularization," *IEEE Trans. Commun.*, vol. 53, no. 1, pp. 195–202, Jan. 2005.

[36] C. Husmann and K. Nikitopoulos, "ViPer MIMO: Increasing large MIMO efficiency via practical vector-perturbation," in *Proc. IEEE Global Commun. Conf. (GLOBECOM)*, Dec. 2018, pp. 1–6.

[37] M. Scalabrin, G. Bielsa, A. Loch, M. Rossi, and J. Widmer, "Machine learning based network analysis using millimeter-wave narrowband energy traces," *IEEE Trans. Mobile Comput.*, vol. 19, no. 5, pp. 1138–1155, May 2020.

[38] H. Huang, Y. Song, J. Yang, G. Gui, and F. Adachi, "Deep-learning-based millimeter-wave massive MIMO for hybrid precoding," *IEEE Trans. Veh. Technol.*, vol. 68, no. 3, pp. 3027–3032, Mar. 2019.

SOHAIL PAYAMI received the M.Sc. degree from Lund University, Sweden, and the Ph.D. degree from the Institute for Communication Systems (ICS), University of Surrey, U.K. He is currently a Researcher with the Institute for Communication Systems and 5G Innovation Centre, University of Surrey. Previously, he was a Research Associate with Heriot–Watt University, U.K. He has worked as a Research Assistant and an Intern with Lund University and the Imperial College London, respectively. His research interests include signal processing for massive MIMO systems, beamforming, and channel modeling.

MOHSEN KHALILY (Senior Member, IEEE) is currently a Lecturer in antenna and propagation with the Home of the 5G Innovation Centre (5GIC), Institute for Communication Systems (ICS), University of Surrey, U.K., where he was a Research Fellow of antennas and propagation, from December 2015 to March 2019. Prior to joining the 5GIC, he was a Senior Lecturer with the Wireless Communication Centre (WCC), University Technology Malaysia (UTM). He has published more than 100 academic articles in international peer-reviewed journals and conference proceedings. His research interests include metasurface engineering, surface electromagnetic, intelligent reflecting surface, phased arrays, hybrid beam-forming, dielectric resonator antennas, leaky wave antennas, and mm-wave and terahertz antennas and propagation. He is a Fellow of the U.K. Higher Education Academy. He is also a member of the IEEE Antennas and Propagation Society, the IEEE Communication Society, and the IEEE Microwave Theory and Techniques Society and an Associate Editor of IEEE Access.

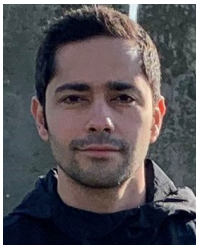

ALI ARAGHI (Senior Member, IEEE) received the M.Sc. degree in electrical engineering-telecommunication-wave from Shahed University, Tehran, Iran, in 2012. He is currently pursuing the Ph.D. degree with the Home of the 5G Innovation Centre (5GIC), Institute for Communication Systems (ICS), University of Surrey, U.K. He worked with the Iran Telecommunication Research Centre (ITRC) as a Research Assistant of antennas and propagation, from 2012 to October 2018. His main research interests include leaky-wave structures, holography theory, metasurfaces, large intelligence surfaces, and the theory of characteristic modes.

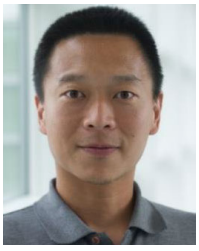

TIAN HONG LOH (Senior Member, IEEE) was born in Malaysia. He received the B.Eng. degree (Hons.) in electrical and electronic engineering from Nottingham Trent University, Nottingham, U.K., in 1999, and the Ph.D. degree in electrical and electronic engineering from the University of Warwick, Coventry, U.K., in 2005. In 2005, he joined the National Physical Laboratory (NPL), Teddington, U.K., as a Higher Research Scientist, and was promoted to a Senior Research Scientist in 2009, and to a Principal Research Scientist, in 2017. He leads work at NPL on a wide range of applied and computational electromagnetic metrology research areas in support of the electronics and communication industry. He holds five patents, four book chapters, and has authored and co-authored over 150 publications. His research interests include metamaterials, computational electromagnetics, small antenna, smart antennas, multiple-input multiple-output (MIMO) antennas, electromagnetic compatibility, body-centric, wireless sensor networks, software-defined radios, and 5G and beyond communications.

DAVID CHEADLE was born in London, U.K. He is currently pursuing the B.Eng. degree in electrical and electronic engineering with London South Bank University. He joined the National Physical Laboratory, Teddington, U.K., as an Assistant Research Scientist, in 2006, and has been promoted to a Research Scientist and a Higher Research Scientist, in 2011 and 2018, respectively. He has over ten years of experience in EMC and antenna metrology. He has been involved in providing measurement services in support of the electronics and communication industry. He currently holds 17 publications. He currently works with the 5G future Communication Technologies Group on research projects related to the measurement of beamforming antennas, fifth-generation and future communication systems, and establishment of wireless communication testbeds using software-defined-radios.

KONSTANTINOS NIKITOPOULOS (Senior Member, IEEE) is currently an Associate Professor of signal processing for communication systems with the Institute for Communication Systems, University of Surrey, Guildford, U.K., and a member of the 5G Innovation Centre (5GIC). He is the Director of the newly established Wireless Systems Laboratory. He also leads the Theory and Practice of Advanced Concepts in Communications Work Area in 5GIC. He has held research positions with RWTH Aachen University, the University of California at Irvine, and the University College London. He was a recipient of the prestigious First Grant of the U.K.'s Engineering and Physical Sciences Research Council and the Principal Investigator of several research projects including AutoAir, a U.K. funded project on 5G Testbeds and Trials. He has been a Consultant for the Hellenic General Secretariat for Research and Technology, where he has also served as a National Delegate of Greece to the Joint Board on Communication Satellite Programs of European Space Agency.

RAHIM TAFAZOLLI (Senior Member, IEEE) has been a Professor of mobile and satellite communications, since April 2000. He has also been the Director of ICS, since January 2010, and the Founder and the Director with the 5G Innovation Centre, University of Surrey, U.K. He has more than 25 years of experience in digital communications research and teaching. He has authored and coauthored more than 500 research publications. He is a co-inventor on more than 30 granted patents, all in the field of digital communications. He is regularly invited to deliver keynote talks and distinguished lectures to International conferences and workshops. In 2011, he was appointed as a Fellow of Wireless World Research Forum (WWRF) in recognition of his personal contributions to the wireless world and the heading one of Europe leading research groups. He is regularly invited by many governments for advice on 5G technologies. He was an Advisor to the Mayor of London in regard to the London Infrastructure Investment 2050 Plan, from May to June 2014. He has given many interviews to international media in the form of television, radio interviews, and articles in international press.